UNCERTAINTY CHARACTERIZATION OF ATMOSPHERIC DENSITY MODELS FOR ORBIT PREDICTION OF SPACE DEBRIS

Luc Sagnières and Inna Sharf

Department of Mechanical Engineering, McGill University, 817 Sherbrooke W., Montreal, QC, H3A 0C3, Canada,
Email: luc.sagnieres@mail.mcgill.ca

ABSTRACT

Atmospheric density modeling represents one of the largest sources of error when determining and propagating the orbit of spacecraft and space debris in low-Earth orbit. In the present work, a framework is developed to characterize the uncertainty due to intrinsic differences between the three emprical atmospheric models most widely used: DTM-2013, NRLMSISE-00, and JB2008. The uncertainty in atmospheric density is modeled using an Ornstein-Uhlenbeck process, a stochastic process adapted for our application in order to understand how the variability of the aforementioned models affect the orbit predictions of satellites. Relevant information for the space debris community is obtained by applying the methodology to the defunct European environmental satellite Envisat, the current target of the European Space Agency's Active Debris Removal mission.

Keywords: atmospheric density, uncertainty characterization, orbit propagation, space debris.

1. INTRODUCTION

For large pieces of space debris, orbiting without the possibility of maneuvering and forever decaying towards Earth, precise knowledge of the evolution of their orbits and related uncertainties is needed to concretely understand the progression and consequences of the space debris problem. As well, predicting the evolution of operational spacecraft trajectories in the long-term requires accurate modeling of the forces affecting their motion. One of the largest sources of uncertainty in spacecraft orbit propagation, especially at low-Earth orbit (LEO) altitudes, arises from the atmospheric drag computation [20]. Some difficulty in attaining truthful forecasts can arise from the calculation of the drag coefficient [15]. However, a large contributor to the total uncertainty is also the errors in atmospheric density modeling [12]. In addition to the difficulties in obtaining accurate solar and geomagnetic indices used in atmospheric models, intrinsic differences in the various modeling techniques provide their own uncertainty in the output of these models.

In the last few decades, empirical atmospheric density modeling has evolved significantly due to the increased availability of satellite data. To date, three comprehensive models have been most widely used: first, the 2013 version of the Drag-Temperature Model (DTM-2013) [3]; second, the Jacchia-Bowman 2008 (JB2008) model [2]; and third the NRLMSISE-00 model developed by the Naval Research Laboratory (NRL) as an extension to Mass Spectrometer and Incoherent Scatter (MSIS) class of atmospheric models [14]. The three models use independent techniques based on various datasets to predict atmospheric densities as a function of location (latitude, longitude, altitude) and time (time of day and of year). Furthermore, different indices for solar and geomagnetic activity are used in the three models. These factors can therefore lead to large discrepencies in the models' density outputs for a specified input time and place.

The aim of the work presented here is to advance our understanding of spacecraft orbit propagation uncertainties and, more specifically, those due to intrinsic differences in atmospheric density modeling. By applying the three models in conjunction during the orbit propagation process, a stochastic framework is developed to characterize the error associated with using any single atmospheric density model output. Modifications to the stochastic process known as the Ornstein-Uhlenbeck process are made and then applied to atmospheric density. Section 2 first dives into the problem of orbit propagation. The various empirical atmospheric models are then discussed and compared in Section 3. The stochastic process used and how it is modified and applied to atmospheric density is described in Section 4. The framework for orbit propagation under aerodynamic drag uncertainties is then outlined in Section 5. Finally, outputs of the framework are displayed in Section 6 for the defunct European environmental satellite Envisat.

2. ORBIT PROPAGATION

Spacecraft orbiting Earth will encounter many perturbing forces, altering their trajectory from a perfectly Keplerian orbit. The dynamics of such a satellite are governed by a differential equation describing the evolution of its position and velocity. In an Earth-centered inertial (ECI) coordinate frame, it is defined as [19]:

$$\ddot{\mathbf{r}}(t) = -\frac{\mu}{r(t)^3}\mathbf{r}(t) + \sum_i \mathbf{a}_i(t, \mathbf{r}(t)) \tag{1}$$

where $\mathbf{r}$ is the position as a function of time t, $r = \|\mathbf{r}\|$, μ is the Earth's gravitational parameter, and $\mathbf{a}_i$ represents the non-gravitational accelerations. The previous equation also assumes a perfectly uniform spherical Earth, and ignores Earth's oblateness and third-body interactions.

A simple model of Earth's gravity is often sufficient, as is the case here, but depending on the application, spherical harmonic models exist to replicate to very high resolution the modifications that need to be made to the gravitational force due to Earth's oblique shape, topographic anomalies, and density variations. Another significant source of orbit perturbations, especially for satellites at geostationary altitudes, is solar radiation pressure (SRP), which has been of interest lately due to the development of solar sails. Other external forces related to SRP include radiation due to Earth's albedo and emissivity and thermal forces from sun-satellite interactions [19]. Similarly to atmospheric density, inaccurate predictions of solar activity is one of the largest sources of error in calculating this effect [19]. The most important perturbing force for Earth-orbiting spacecraft in LEO is, however, the aerodynamic drag.

Aerodynamic drag is caused by particles interacting with the satellite body creating an acceleration in the opposite direction of its motion. As the Earth's atmosphere can extend up to an altitude of 1000 km, it needs to be considered for most satellites in LEO, especially for satellites with large surface areas. Understanding aerodynamic drag requires an accurate knowledge of the atmosphere, the spacecraft surfaces, and how the spacecraft interacts with the atmosphere. The standard equation describing the acceleration due to aerodynamic drag, $\mathbf{a}_{\text{drag}}$, is as follows [19]:

$$\mathbf{a}_{\text{drag}} = -\frac{1}{2}\frac{c_D A}{m}\rho \dot{r}_{\text{rel}}^2 \frac{\dot{\mathbf{r}}_{\text{rel}}}{\|\dot{\mathbf{r}}_{\text{rel}}\|} \tag{2}$$

where c_D is the drag coefficient, A is the satellite cross-sectional area normal to the incident flow, m is the spacecraft mass, ρ is the atmospheric density, and $\dot{\mathbf{r}}_{\text{rel}}$ is the relative velocity of the satellite with respect to the atmosphere. In the present work, the atmosphere is assumed to be co-rotating with Earth.

Accurately computing the aerodynamic drag on a satellite is important to predict that satellite's lifetime. A few decades ago, it was found that none of the atmospheric models available at the time could correctly be used to deduce the influence of satellite drag on orbital motion [8]. The same is true today, although to a lesser degree: uncertainties in modelling aerodynamic drag can have dangerous consequences on the expected lifetime of LEO spacecraft and these uncertainties emerge from a large variety of places. As described in [20], errors in computing the effect of satellite drag can come from the wrong use of atmospheric models, uncertainties related to them, or inherent unknowns in satellite parameters, among others.

One of the largest sources of errors in the calculation of aerodynamic drag is the drag coefficient, c_D. Historically, an accepted value of 2.2 was used and no further effort was deemed necessary as atmospheric models were still very uncertain [4]. Now that atmospheric density models are more precise, more effort has been made to reduce errors in c_D. Multiple methods, either analytical or numerical, exist for measuring the interaction between atmospheric flow and specific geometric surfaces, and a rough bound for the drag coefficient is between 2 and 4, depending on shape, altitude, and molecular content [15, 20, 9]. In addition to errors in c_D, uncertainties in atmospheric densities will also strongly influence the calculation of aerodynamic drag.

Many attempts at describing random fluctuations and uncertainties associated with atmospheric density and therefore aerodynamic drag have been made since the early 1960s. A first study looked at errors in orbit predictions by separating drag fluctuations into a sinusoidal component and random fluctuations [13]. In a later study, the effect of drag on the orbital elements was modeled by considering random fluctuations in drag as a stochastic process known as the Ornstein-Uhlenbeck process and the improvement of the stochastic model was highlighted when applied to a specific satellite, 1960 Omicron [16]. In addition, the author suggested modifying the stochastic process to improve its accuracy [16]. In a study of torques experienced by satellites, variations of atmospheric density were modeled as white noise in the stochastic differential equation for attitude motion of a spacecraft experiencing gravity gradient and aerodynamic torques [17]. A stochastic model for atmospheric density was also developed incorporating variations in local atmospheric densities as a second-order stochastic Taylor expansion in powers of zero-mean Gaussian random variables [5].

The most complete study into the stochasticity of aerodynamic drag, its source, and its effect on orbital parameters, though, has been carried out recently by the authors of [6]. They developed expressions for the relation between errors in atmospheric density and errors in mean anomaly, related to the in-track position, and mean motion, related to the semi-major axis (SMA). By comparing density forecasts driven by solar extreme ultraviolet (UEV) irradiance to stochastic models for atmospheric density using white noise and Brownian motion, they showed that Brownian motion closely approximates the error in EUV forecasts, and therefore forecast errors in mean anomaly and mean motion grow as t^5 and t^3, respectively, due to uncertainty in solar irradiance.

All of these studies have tried to capture the uncertainty associated with random fluctuations in atmospheric density. However, quantifying concretely the intrinsic differences between the state-of-the-art atmospheric models and how they contribute to uncertainties in orbit propagation has not been done to date. This study provides a first glance into how to deal with this issue.

3. ATMOSPHERIC DENSITY MODELING

The atmosphere, and in particular atmospheric densities at satellite altitudes, are constantly evolving. Density decreases exponentially with altitude, and changes in geomagnetic and solar activity can cause large density variations on top of seasonal and diurnal effects. There exists a large variety of atmospheric models but the most commonly used empirical models of the upper atmospheric are DTM-2013, JB2008, and NRLMSISE-00 [3, 2, 14]. A recent and comprehensive review of atmospheric density modeling can be found in [7].

3.1. Empirical Atmsopheric Density Models

Originally developed in 1978, DTM is a three-dimensional thermospheric model based on the diffusive equilibrium and spherical harmonics of individual atmospheric constituents combined with satellite drag data and in-situ measurements. New data and improvements of the algorithms, leading to better agreements for extreme solar and geomagnetic conditions, were added in later versions and further improvements were made by including incoherent scatter radar and satellite interferometer data as well as different proxies for solar activity. The latest version, released as DTM-2013, includes a large dataset from GRACE, CHAMP and the GOCE satellite and uses F30 as a solar activity proxy, covering the 200-900 km altitude range and using K_p as its geomagnetic index [3].

The Jacchia atmospheric models solve the diffusion equation to obtain temperature, density and composition data from 90 km to 2500 km [10]. Systematic variations with the solar cycle, with solar activity over one solar rotation, semiannual variations, seasonal-latitudinal variations, diurnal variations, variation with geomagnetic activity and rapid fluctuations from gravity waves are deduced from satellite drag data and are also taken into account in the model equations. Improvements were made over the years by improving the boundary conditions of the diffusion equations and with new satellite data.

The Jacchia-Bowman 2008 (JB2008) model improves on the Jacchia models by incorporating new solar indices obtained from on-orbit sensor data and using a new semiannual density model and geomagnetic index model with temperature correction equations for high altitudes up to 4000 km [2]. Furthermore, JB2008 includes more data sources such as daily density values from drag analysis of numerous satellites, accelerometer data from CHAMP and GRACE as well as density values from the High Accuracy Satellite Drag Model (HASDM) [18].This model uses as input a combination of solar parameters ($F_{10.7}$, S_{10}, M_{10}, Y_{10} and their 81-day centered averages with 1, 1, 2, and 5-day lags, respectively) and the Dst geomagnetic index [2].

The third category, the MSIS-class models differ from the Jacchia models in that they are thermospheric models based directly on measurements of atmospheric densities from satellites and temperatures obtained from incoherent scatter measurements at ground stations. A major upgrade to the MSIS-class of models is the more recent NRLMSISE-00 model. In addition to a more extensive data set in spatial range and time period, the model also includes the satellite drag data which are the basis of the Jacchia models, bringing forward the advantages of both types of models. Furthermore, NRLMSISE-00 includes the effect of anomalous oxygen (O^+ and hot atomic oxygen) in the mass density above 500 km, an important component to satellite drag at these altitudes [14]. Space weather inputs include the previous day observed $F_{10.7}$, the 81-day centered average $F_{10.7}$ and the 3-hour magnetic index a_p. The outputs are two temperature values—the local neutral temperature and the asymptotic value at the exosphere, i.e., exospheric temperature—as well as number densities for various neutral species, anomalous oxygen and the total mass density.

3.2. Comparison of Model Outputs

Although all these models have their benefits and limitations, large uncertainties are present and should be kept in mind when using them [20]. While authors might produce standard deviation errors or mean residuals for their models, the accuracy is often biased towards the altitude range and time period of the satellite data from which the model was developed [20]. Early models were shown to give mean values typically within 10% of observational data with standard deviations of approximately 15% [12]. Nevertheless, the JB2008 model claims to have standard deviations of approximately 10% at 400 km, while authors of DTM2013 claim that their model is more accurate than JB2008 at all altitudes [2, 3]. In general, a 10-15% accuracy should be assumed, although that can be much higher for short-term and local variations [20].

A better comprehension of the discrepancies between models can be obtained by considering a globally-averaged density profile for a specific altitude and time frame, as for example, is shown in Fig. 1 for 400 km using inputs for the year 2014. The globally-averaged density was obtained by discretizing Earth into 5° latitude by 5° longitude bins and averaging the density values at each bin, weighing them according to their surface area. One can see that the density profiles share a similar shape; however, differences of up to a factor of 2 are present for short time periods.

Propagating orbits by using the atmospheric densities from each model will also lead to diverging orbit parameters as the instantaneous differences accumulate over time. Fig. 2 shows the change in SMA for a spacecraft in Envisat's orbit with a cross-sectional area of 10 m^2 when propagating its polar orbit using each atmospheric density model for 2014 (solid lines), following the propagation method explained in Section 5. Envisat is assumed to be in a polar orbit at an altitude of 765 km, an inclination of 98.3°, and an eccentricity of 10^{-4}. After one year, a difference of over 30% is present between the change

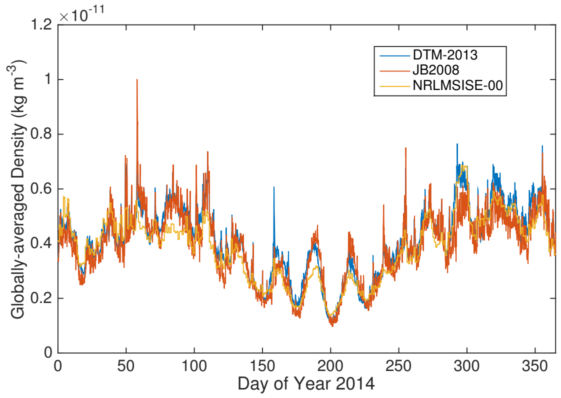

Figure 1. Globally-averaged atmospheric density at 400 km for 2014

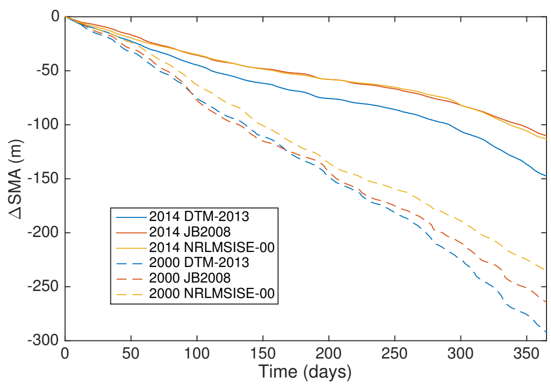

Figure 2. Change in SMA for Envisat's orbit

in SMA that used DTM-2013 and the one from the other two models. This is due to DTM-2013 atmospheric densities being higher than the other two models for Envisat's orbit. The same analysis for the year 2000 (dashed lines) demonstrates up to a 25% difference in SMA change after one year between the smallest and largest predictions. The differences witnessed in these examples suggest a need for quantifying the uncertainty in atmospheric density predicted by the three models.

4. DENSITY VARIATIONS AS A STOCHASTIC PROCESS

4.1. Stochastic Processes

A stochastic process is a collection of random variables that evolve with time. Unlike a deterministic process, which has a unique solution, a stochastic process can expand into infinitely many paths. The most well known stochastic process is the Wiener process, also known as standard Brownian motion, and is most commonly used to describe uncertainties in dynamical systems as it is the integral of ideal white noise. A Wiener process, $W = \{W_t, t \geq 0\}$, is a continuous stochastic process that has independent increments which follow the same Gaussian distribution [11].

Another stochastic process, also commonly used to describe the physics of Brownian motion, is the Ornstein-Uhlenbeck process [11]. It has been applied to describe the velocity of Brownian particles undergoing friction and is dependent on the Wiener process. The key property of the Ornstein-Uhlenbeck process is that it is mean-reverting: there is a long-term tendency to drift towards a mean value. It is often used in economics to stochastically model interest rates, currency exchange rates and commodity prices. The stochastic differential equation (SDE) defining the Ornstein-Uhlenbeck process X_t is as follows [11]:

$$dX_t = \theta(\mu - X_t)dt + \sigma dW_t \tag{3}$$

where θ is defined as the speed of reversion, μ is the mean, and σ is the instantaneous volatility. A larger θ increases the speed at which X_t reverts back to its mean μ. A larger σ increases the intensity of the fluctuations. The long-term variance of the process is defined by its two parameters [11]:

$$Var(X_t) = \sigma^2/2\theta \tag{4}$$

4.2. Ornstein-Uhlenbeck Process for Atmospheric Density Modeling

An Ornstein-Uhlenbeck process with time-dependent parameters can also be defined, where μ, σ, and even θ can be considered to vary as a function of time. This process is often used in statistics in the context of degradation processes and survival analysis. A more general SDE with time-dependent parameters can therefore be defined as follows:

$$dX_t = \theta_t(\mu_t - X_t)dt + \sigma_t dW_t \tag{5}$$

In such a process, the long-term variance, defined by Eq. (4) for a standard Ornstein-Uhlenbeck process, will also become time-dependent, as follows:

$$s_t^2 = \sigma_t^2/2\theta_t \tag{6}$$

with s_t being the long-term time-dependent standard deviation.

Atmospheric density at a certain geographic position follows daily cycles due to the sun's influence on the expansion and compression of the atmosphere as it heats and cools. Similarly, as a spacecraft orbits Earth, it will witness orbital cycles in the atmospheric densities it encounters, and those cycles will evolve over time. Two further modifications to the general time-dependent Ornstein-Uhlenbeck process are proposed here for describing this evolution: first, a tendency to follow the varying mean; and second, the additional property of keeping the proportional distance to the mean and standard deviation the same as in the standard Ornstein-Uhlenbeck process.

The main effect of the first modification is that, for any point in time, the distance between the sample path of the process and the mean is the same as the standard Ornstein-Uhlenbeck process. The advantage of this modification is that if any large, or cyclic, variations are present, as is the case for atmospheric density, then instead of simply drifting towards the mean, the process will also follow the fluctuations, keeping the evolutions of both the process and the mean in agreement.

The second modification seeks to control the fluctuations of the process in order to keep the proportional distance to the mean and standard deviation the same as for the standard Ornstein-Uhlenbeck process, for any point in time. The advantage of this is similar to the advantage of the first modification. It will follow more closely the relative path of the standard Ornstein-Uhlenbeck process when compared to its mean and standard deviation. In the long-term, the general time-dependent Ornstein-Uhlenbeck process (Eq. (5)) can drift to larger distances away from the mean than the process with the two modifications, not representative of the properties of the standard Ornstein-Uhlenbeck process (Eq. (3)).

Combining the two changes, we arrive at a modified Ornstein-Uhlenbeck process with time-dependent parameters. The SDE describing this process is as follows:

$$dX_t = \theta_t(\mu_t - X_t)dt + \sigma_t dW_t + d\mu_t + \frac{X_t - \mu_t}{s_t} ds_t \quad (7)$$

where the third and fourth term on the right-hand side represent the first and second modifications proposed, respectively.

The modified Ornstein-Uhlenbeck stochastic process can be applied to atmospheric density, and in particular, to orbit propagation due to atmospheric drag, by considering the sample path of the process as the atmospheric densities experienced during the satellite trajectory throughout the propagation period. The modified Ornstein-Uhlenbeck process can also be applied to study the influence of the uncertainty in a specific model by using the calculated value from that model and its claimed accuracy for μ_t and s_t, respectively. However, the object of this study is to determine the effect of the uncertainty due to the intrinsic differences between the three models summarized in Section 3. This can therefore be measured by considering μ_t as the mean at every point in time of the three atmospheric density models, DTM-2013, JB2008, and NRLMSISE-00, and s_t as their standard deviation. In doing so, the stochastic framework implicitly assumes that no single atmospheric model is more accurate than the others and that the uncertainty in the atmospheric density is in fact captured by the differences between the models. Unlike μ and s, which are obtained directly from the models, θ is a property of the Ornstein-Uhlenbeck process and can therefore be kept constant. When applied to atmospheric density, Eq. (7) now becomes:

$$d\rho_t = \theta(\mu_t - \rho_t)dt + \sigma_t dW_t + d\mu_t + \frac{\rho_t - \mu_t}{s_t} ds_t \quad (8)$$

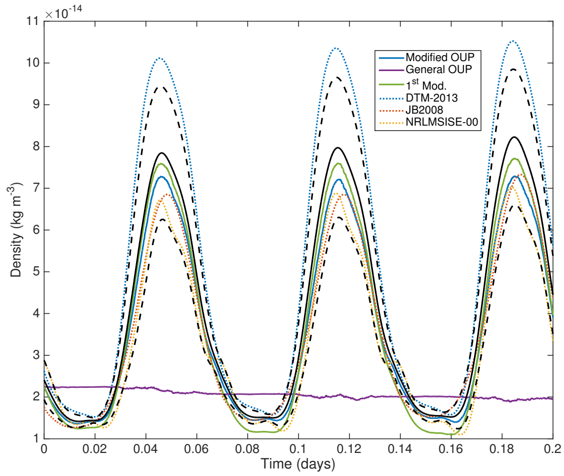

Figure 3. Ornstein-Uhlenbeck process applied to atmospheric density

An example sample path of the Ornstein-Uhlenbeck process using Eq. (8) can be found in Fig. 3. The orbit of Envisat was propagated for 0.2 days ($\approx$ three orbits) using the mean atmospheric density from the three models (solid black line) to calculate aerodynamic drag. The dashed black lines represent $\mu \pm s$ and the dotted lines represent the densities from each model. In parallel, Eq. (8) was propagated to obtain a sample path of the density, shown by the light blue solid line. To emphasize the need for the two modifications to the stochastic process, a sample path solution using the SDE in Eq. (5) instead of Eq. (8) is shown by the purple line, while a sample path solution using only the first, but not second modification, is shown by the green line. One can see how the green line diverges from the mean value for low densities even though the three models are in close agreement. The same random increments generated by the Wiener process are kept for the three sample paths to emphasize the difference between each process.

A value for θ of 10^{-6} was chosen for the results presented in Fig. 3: using another value of θ does not only change the speed at which the random variable reverts back to the mean, it also changes the value of the instantaneous volatility, σ_t, since the long-term variance in Eq. (6), s_t^2, is fixed by the values of atmospheric density found in the three models. Therefore, an increase in θ leads to an increase in the instantaneous volatility. Larger θ values displayed too strong fluctuations in density not representative of actual density variations. On the other hand, smaller values of θ led to slower and smaller drifts in the observed trend, an indication of the worst-case scenario when larger departures from the mean are kept for longer periods of time. A sensitivity study on this parameter can be found in Section 6. In the following section, the numerical integration method is explained, where, unlike for the results in Fig. 3, the value of density from the sample path will be used to compute the orbit. The mean density was used here in order to provide a valid and meaningful comparison between the sample paths.

5. STOCHASTIC ORBIT PROPAGATION

Now that a stochastic process for atmospheric density has been determined, the SDE displayed in Eq. (8) can be coupled with the differential equation defining a satellite's orbit in Eq. (1), assuming aerodynamic drag is the only non-gravitational acceleration:

$$\ddot{\mathbf{r}}(t) = -\frac{\mu}{r(t)^3}\mathbf{r}(t) - \frac{1}{2}\frac{c_D A}{m}\rho_t \dot{r}_{\text{rel}}^2 \frac{\dot{\mathbf{r}}_{\text{rel}}}{||\dot{\mathbf{r}}_{\text{rel}}||} \tag{9}$$

Eqs. (8) and (9), propagated alongside one another, define the developed framework for the uncertainty characterization of aerodynamic drag and its effect on orbital propagation due to intrinsic differences in empirical atmospheric models.

Recently, numerical solutions to SDEs have quickly been expanding because of increasing computational power and the fact that most typical integration methods perform poorly when applied to SDEs [11]. The Milstein method is one of the most simple, yet effective, integration methods for SDEs [11]. For an SDE of the form:

$$dX(t) = a(X,t)dt + b(X,t)dW_t \tag{10}$$

the Milstein algorithm takes the form [11]:

$$\begin{aligned} x_{i+1} &= x_i + a(t_i, x_i)\Delta t_{i+1} + b(t_i, x_i)\Delta W_{i+1} \\ &+ \frac{1}{2}b(t_i, x_i)\frac{\partial b}{\partial x}(t_i, x_i)(\Delta W_{i+1}^2 - \Delta t_{i+1}) \end{aligned} \tag{11}$$

with $\Delta W_i = z_i\sqrt{\Delta t_i}$ and where z_i is chosen randomly from $N(0,1)$. Applying the Milstein method to Eq. (8), and noting that there is no dependence of the $b(x,t)$ term on x in our case, gives:

$$\begin{aligned} \rho_{i+1} &= \rho_i + \theta(\mu_i - \rho_i)\Delta t_{i+1} + \sigma_i \Delta W_{i+1} \\ &+ \Delta\mu_{i+1} + \frac{\rho_i - \mu_i}{s_i}\Delta s_{i+1} \end{aligned} \tag{12}$$

This method is first-order, and higher order methods were not attempted due to their dependence on atmospheric density values at intermediate time steps, and hence, more evaluations of the three atmospheric models leading to much longer computation times.

The framework revolves around propagating the coupled Eqs. (8) and (9) in parallel. The first-order ODE in Eq. (9) is integrated forward by using the desired numerical integration method and assuming constant atmospheric density over the time step to manage computation times. The Runge-Kutta Dormand-Prince (RKDP) solver was used for the results presented in Section 6 with a time step of 1 s. Atmospheric densities from the three models, their mean and their standard deviation are determined using $\mathbf{r}(t)$ and $\dot{\mathbf{r}}(t)$ at every time step and Eq. (12) can then be applied. The initial density ρ_0 was calculated to include an initial uncertainty as follows:

$$\rho_0 = \mu_0 + z_0 s_0 \tag{13}$$

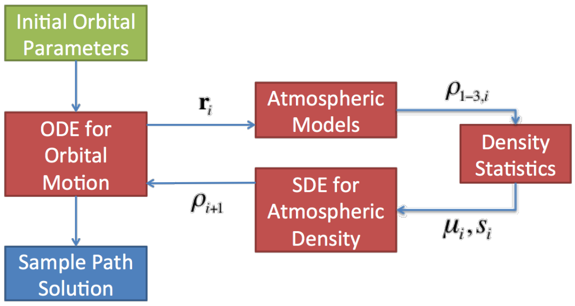

Figure 4. Flowchart of the algorithm

where z_0 is chosen from $N(0,1)$ and s_0 is the standard deviation of the densities from the three models at the initial position. The normally distributed random number with zero mean and unit variance can be obtained using the Box-Muller transform. Using a pseudo-random number generator, one can obtain two random numbers, u_1 and u_2, uniformly distributed between 0 and 1, and transform them into a normally distributed random value, z, in the following way:

$$z = \cos(2\pi u_1)\sqrt{-2\ln u_2} \tag{14}$$

Eqs. (8) and (9) are propagated for the desired period of time. The entire process is repeated 1000 times in a Monte Carlo simulation in order to obtain probability distributions for the orbital parameters over the time frame. The complete framework is represented in a flowchart in Fig. 4: the input is the initial orbital parameters; the output of the procedure are the sample paths for the orbital parameters, as well as their probability distribution over time from the Monte Carlo simulation.

6. RESULTS

The simulation was performed for Envisat for the year 2000, that is, using the solar indices measured during that year as input to the three atmospheric models. A value of 2.2 was adopted for c_D, an approximate constant cross-sectional area of 10 m^2 was assumed, and a mass of 7828 kg was chosen [4, 1]. Furthermore, Envisat's orbital parameters as presented in Section 3.2 were set as the initial conditions.

The orbital parameters that are most affected by aerodynamic drag and its variability are the SMA and the mean anomaly [6]. Indeed, no significant changes in eccentricity, inclination, or right ascension of the ascending node were found in any of the simulations. As we are concerned with the changes in the orbit and not the position of the satellite within its orbit, only the SMA solutions will be considered.

Fig. 5 shows the evolution of the probability density function (PDF) for the change in SMA every two months for the runs with $\theta = 10^{-6}$. As can be expected, the distribution widens over time: a mean monthly decrease of

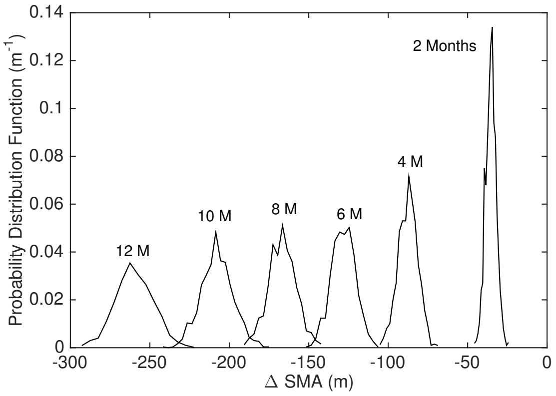

Figure 5. Evolution of the PDFs for the change in SMA at two-month intervals

approximately 22 m is observed, with a mean decrease of 260 m after one year, while the standard deviation of the distribution ranges from 2 m after one month to 12 m after one year.

A useful parameter to measure the uncertainty on the change in SMA in the propagation is the coefficient of variation, c_V, also known as the relative standard deviation; it is a measure of the dispersion of a probability distribution, and is defined as:

$$c_V = \frac{\sigma}{|\mu|} \tag{15}$$

with μ being the mean of the distribution and σ its standard deviation. The advantage of using this value, instead of the regular standard deviation, is its ability to provide comparable information between different probability distributions. While a standard deviation usually only provides information in the context of its dataset and the mean associated with it, the coefficient of variation can be used to compare distributions over time, and here, even to compare various simulations.

A sensitivity study on θ was performed in order to understand the dependence of the framework on this parameter. Fig. 6 displays the evolution of the coefficient of variation for each of the Monte Carlo simulations with a particular value of θ. These results show how modifying the speed of reversion θ changes the evolution of the coefficient of variation. In this case, the mean decrease in SMA was the same for all the value of θ considered (seen in Fig. 5 for $\theta = 10^{-6}$), but the standard deviation soared for smaller values of θ, leading to higher values of the coefficient of variation. A feature that is repeated in most of the c_V profiles is that the coefficient of variation decreases with time, unlike the standard deviation. The starting value of the coefficient of variation after one day for all of the cases is approximately 15%, and it varies to approximately 2, 4, 12, and 17% after one year for θ values of 10^{-5}, 10^{-6}, 10^{-7}, and 10^{-8}, respectively.

As previously mentioned, a θ value of 10^{-5} displayed fluctuations not physically representative of actual density variations, while a value of 10^{-8} represents the worst-case scenario, when larger departures from the mean persist for longer periods of time. For comparison, the coefficient of variation and its evolution were also calculated from the three deterministic orbital propagations, each computed with one of the three atmospheric models as seen in Fig. 2. The value of μ was taken as the mean of the three decreases in SMA and σ as their standard deviation and the corresponding result for c_V is also plotted in Fig. 6. In this case, the coefficient of variation of the orbital decay from the three models varies more significantly than for the framework results, decreasing for half of the year from 15 to 4% and then increasing to 9% after one year. It can be concluded that the developed framework provides a more accurate quantification of the uncertainty than the orbit propagation using each model separately as the Monte Carlo simulation will consider every plausible scenario. For example, if the three profiles of the SMA changes incidentally cross paths at some point, the coefficient of variation calculated from the three models would be small (0 at the crossing point), while the Monte Carlo simulation using the modified Ornstein-Uhlenbeck process would provide a much larger and more realistic uncertainty estimate.

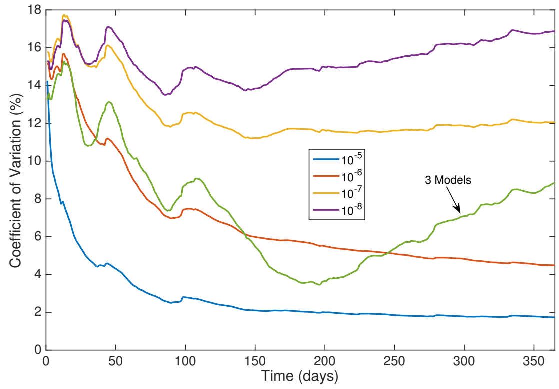

Figure 6. Evolution of the coefficient of variation

7. CONCLUSION

In this work, the three most widely-used empirical atmospheric density models were compared and a framework was developed to characterize the uncertainty in orbit propagation due to their intrinsic differences in atmospheric density modeling. The stochastic process known as the Ornstein-Uhlenbeck process is described, and two modifications are outlined for its application to atmospheric density stochastic modeling. The propagation method, which makes use of the three atmospheric models in conjunction, is detailed, and the framework is applied to the defunct European satellite Envisat.

It was shown that the developed framework was more appropriate to measure the uncertainty in orbit propagation due to aerodynamic drag than simply comparing the propagated orbits that used individual atmospheric models. However, a strong dependence of the stochastic framework on its θ parameter was noticed. A worst-case scenario, obtained by fixing $\theta = 10^{-8}$, showed twice the uncertainty after one year, at 17%, than the relative standard deviation from the three individual models, at 9%. On the other hand, using a value of $\theta = 10^{-6}$ resulted in uncertainty on the change in SMA that decreased to 4% after one year.

The uncertainties computed here in orbit propagation would come on top of uncertainties in aerodynamic drag arising from other sources, such as the unpredictability of the solar flux. A sensitivity study on orbital parameters and other initial conditions could also be performed. It would provide the results needed to develop an appreciation of the framework for different applications. This methodology could also be used to gain insight into individual atmospheric models. By applying the described method to a single model with uncertainties for that model's input parameters, uncertainties on the model outputs and their effect on orbit propagation could be assessed. Furthermore, although only the semi-major axis was considered here, analyses on the mean anomaly of satellites could also be done. Finally, information on the rotational dynamics of spacecraft could be obtained by coupling attitude propagation to the framework and including the influence of the aerodynamic torque.

ACKNOWLEDGMENTS

This work was supported by Hydro-Québec through the McGill Engineering Doctoral Award. The authors are further grateful for the support of Natural Sciences and Engineering Research Council of Canada (NSERC). Computations were made on the supercomputer Guillimin from McGill University, managed by Calcul Québec and Compute Canada. The operation of this supercomputer is funded by the Canada Foundation for Innovation (CFI), ministère de l'Économie, de la Science et de l'Innovation du Québec (MESI) and the Fonds de recherche du Québec - Nature et technologies (FRQ-NT).

REFERENCES

1. Bastida Virgili B., Lemmens S., Krag H., (2014). Investigation on Envisat Attitude Motion, e.Deorbit Workshop, European Space Agency, The Netherlands.
2. Bowman B.R., Tobiska W.K., Marcos F.A., et al., (2008). A new empirical thermospheric density model JB2008 using new solar and geomagnetic indices, In: AIAA/AAS Astrodynamics Specialist Conference, 18-21 August 2008, Honolulu, Hawaii, paper AIAA 2008-6438.
3. Bruinsma S. L., (2015). The DTM-2013 thermosphere model, *J. Space Weather Space Clim.*, 5, A1. http://dx.doi.org/10.1051/swsc/2015001.
4. Cook G.E., (1965). Satellite drag coefficients, *Planetary and Space Science*, 13, 929-946.
5. de Lafontaine J., (1990). Orbital dynamics in a stochastic atmosphere, *Journal of Guidance, Control, and Dynamics*, 13(3), 483-491.
6. Emmert J. T., Warren H. P., Segerman A. M., et al., (2017). Propagation of atmospheric density errors to satellite orbits, *Adv. Space Res.*, 59, 147-165.
7. Emmert J. T., (2015). Thermospheric mass density: A review, *Advances in Space Research*, 56, 773-824.
8. Gaposchkin E. M., Coster A. J., (1988). Analysis of satellite drag, *Lincoln Laboratory Journal*, 1(2), 203-224.
9. Gaposchkin E. M., (1994). Calculation of satellite drag coefficients, Technical Report 998, MIT Lincoln Laboratory, Lexington, MA.
10. Jacchia L.G., (1965). Static diffusion models of the upper atmosphere with empirical temperature profiles, *Smithsonian Contr. Astrophys.*, 8, 215-257.
11. Kloeden P. E., Platen E., (1999). *Numerical Solution of Stochastic Differential Equations*, Springer-Verlag Berlin Heidelberg, Third Edition.
12. Marcos F.A., (1990). Accuracy of atmosphere drag models at low satellite altitudes, Âdv. Space Res., 10 (3), 417-422.
13. Moe K., (1962). Stochastic models of the errors in orbital predictions for artificial Earth satellites, *ARS Journal*, 32, 1726-1728.
14. Picone J.M., Hedin A.E., Drob D.P., et al., (2002). NRLMSISE-00 empirical model of the atmosphere: statistical comparisons and scientific issues, *J. Geophys. Res.*, 107. http://dx.doi.org/10.1029/2002JA009430.
15. Prieto D. M., Graziano B. P., and Roberts P. C., (2014). Spacecraft drag modelling, *Progress in Aerospace Sciences*, 64, 56-65.
16. Rauch H. E., (1965). Optimum Estimation of Satellite Trajectories Including Random Fluctuations in Drag, *AIAA Journal*, 3(4), p. 717.
17. Sagirow P., (1970). Stochastic Methods in the Dynamics of Satellites, *ICMS Lecture Notes*, 57, doi:10.1007/978-3-7091-2870-1.
18. Storz F., Bowman B., Branson J.I., et al., (2005). High accuracy satellite drag model (HASDM), *Advances in Space Research*, 36, 2497-2505.
19. Vallado D., (2013). *Fundamentals of Astrodynamics and Applications*, Microcosm, Hawthorne, CA.
20. Vallado D., Finkleman D., (2014). A critical assessment of satellite drag and atmospheric density modelling, *Acta Astronautica*, 95, 141-165.